Available online at www.sciencedirect.com
SciVerse ScienceDirect
Procedia Computer Science 18 (2013) 889 – 898
Procedia Computer Science

2013 International Conference on Computational Science

Multi-level CFD-based Airfoil Shape Optimization with Automated Low-fidelity Model Selection

Slawomir Koziel[a*] and Leifur Leifsson[a]

[a]*Engineering Optimization & Modeling Center, School of Science and Engineering, Reykjavik Uni., Menntavegur 1, 101 Reykjavik, Iceland*

Abstract

Computational fluid dynamic (CFD) models are ubiquitous in aerodynamic design. Variable-fidelity optimization algorithms have proven to be computationally efficient and therefore suitable to reduce high CPU-cost related to the design process solely based on accurate CFD models. A convenient way of constructing the variable-fidelity models is by using the high-fidelity solver, but with a varying degree of discretization and reduced number of flow solver iterations. So far, selection of the appropriate parameters has only been guided by the designer experience. In this paper, an automated low-fidelity model selection technique is presented. By defining the problem as a constrained nonlinear optimization problem, suitable grid and flow solver parameters are obtained. Our approach is compared to conventional methods of generating a family of variable-fidelity models. Comparison of the standard and the proposed approaches in the context of aerodynamic design of a transonic airfoil indicates that the automated model generation can yield significant computational savings.

Keywords: Aerodynamic design, multi-level algorithm, low-fidelity model selection, numerical optimization.

1. Introduction

High-fidelity computational fluid dynamic (CFD) models are an integral part of contemporary aerodynamic shape design [1,2]. Direct optimization of the high-fidelity CFD model is often impractical due to high computational cost of each simulation and the fact that conventional optimization methods (e.g., gradient-based, or population-based) normally require large number of objective function evaluations to yield an optimized design [3-6]. This problem can be partially alleviated using cheap adjoint sensitivity [1]. However, this technology is not always available, and, the number of required CFD simulations may still be prohibitively large.

The aerodynamic design process can be accelerated by means of surrogate-based optimization (SBO) [3-5]. The overall objective of SBO is to reduce the number of evaluations of the high-fidelity models, and it is achieved by using computationally cheap surrogate functions in lieu of the computationally more expensive high-fidelity models. SBO with physics-based surrogate models was shown to very effective in aerodynamic

* Corresponding author. Tel.: +354-599-6376 ; fax: +354-599-6489;
E-mail address: koziel@ru.is

Selection and peer review under responsibility of the organizers of the 2013 International Conference on Computational Science
doi:10.1016/j.procs.2013.05.254

shape optimization [6-10]. In particular, for CFD-based shape optimization, low-fidelity models based on the same flow solver as the high-fidelity one but with coarser discretization and reduced flow solver iterations (so-called variable-resolution SBO) are found to be both efficient and reliable [6,10]. The difficulty in using those types of methods lies in the selection of the discretization parameters and the flow solver convergence criteria. This process is currently hands-on and guided by engineering experience.

In this paper, we present an automated way of setting up the low-fidelity models. In particular, we formulate the problem as a constrained nonlinear optimization problem and use numerical techniques to find the appropriate values of the model discretization parameters. The proposed technique replaces the ad-hoc method of constructing the low-fidelity models, and, consequently, automates the entire process. At the same time, it provides more accurate and reliable models. Application to the aerodynamic design of transonic airfoils and comparison with the conventional approach is provided.

2. Aerodynamic Shape Optimization by Multi-level CFD Models

In this section, we formulate the aerodynamic shape design problem. We also describe a recently introduced variable-fidelity solution approach [11], which exploits a set of CFD models of increasing discretization density–so-called multi-level optimization algorithm.

2.1. Problem Formulation

Airfoil shape optimization aims at obtaining a geometry which provides a certain aerodynamic performance, e.g., minimum drag for a given lift. The problem can be formulated as a constrained nonlinear minimization, i.e., for a given set of operating conditions, solve

$$\begin{aligned} &\min_{\boldsymbol{x}} f(\boldsymbol{x}) \\ &s.t.\ g_j(\boldsymbol{x}) \le 0,\ j = 1,\ldots,M \\ &\quad h_k(\boldsymbol{x}) = 0,\ k = 1,\ldots,N \\ &\quad \boldsymbol{l} \le \boldsymbol{x} \le \boldsymbol{u} \end{aligned} \tag{1}$$

where $f(\boldsymbol{x})$ is the objective function, $\boldsymbol{x}$ is the design variable vector describing the airfoil shape, $g_j(\boldsymbol{x})$ are the inequality constraints, M is the number of the inequality constraints, $h_k(\boldsymbol{x})$ are the equality constraints, N is the number of the equality constraints, and $\boldsymbol{l}$ and $\boldsymbol{u}$ are the design variables lower and upper bounds, respectively. It is assumed that the objective and constraint functions are obtained by a high-fidelity CFD solver. The objective can be, for example, $f(\boldsymbol{x}) = C_d(\boldsymbol{x})$ with the constraints $g_1(\boldsymbol{x}) = C_{l.\min} - C_l(\boldsymbol{x}) \le 0$ and $g_2(\boldsymbol{x}) = A_{\min} - A(\boldsymbol{x}) \le 0$, where C_d is the drag coefficient, C_l is the lift coefficient, $C_{l.min}$ is a minimum allowable lift coefficient, A is the cross-sectional area, and A_{min} is a minimum allowable cross-sectional area.

2.2. Multi-level Optimization Algorithm

A multi-level optimization algorithm is adopted here to solve (1). The algorithm was first introduced in the area of microwave engineering [12], and later applied to airfoil shape optimization [11]. The algorithm exploits a family of low-fidelity models denoted as $\{c_j\}$, $j = 1, \ldots, K$, all evaluated by the same CFD solver as the one used for the high-fidelity model f. Discretization of the model c_{j+1} is finer than that of the model c_j, which results in a better accuracy but also a longer evaluation time. In practice, $K = 2$ or 3. The discretization density may be controlled by solver-dependent parameters (e.g., the meshing parameters).

The multi-level optimization works as follows. Starting from the initial design $\boldsymbol{x}^{(0)}$, the coarsest model c_1 is optimized to produce a first approximation of the high-fidelity model optimum, $\boldsymbol{x}^{(1)}$. The vector $\boldsymbol{x}^{(1)}$ is used as a

starting point to find the next approximation of the high-fidelity model optimum, $\boldsymbol{x}^{(2)}$, which is obtained by optimizing the next model, c_2. The process continues until the optimum $\boldsymbol{x}^{(K)}$ of the last low-fidelity model c_K.

Having $\boldsymbol{x}^{(K)}$, we evaluate the model c_K at all perturbed designs around $\boldsymbol{x}^{(K)}$, i.e., at $\boldsymbol{x}_k^{(K)} = [\boldsymbol{x}_1^{(K)} \ldots \boldsymbol{x}_k^{(K)} + \text{sign}(k)\cdot d_k \ldots \boldsymbol{x}_n^{(K)}]^T$, $k = -n, -n+1, \ldots, n-1, n$. We use the notation $c^{(k)} = c_K(\boldsymbol{x}_k^{(K)})$. This data is used to refine the final design without directly optimizing the high-fidelity model f. More specifically, we set up an approximation model involving $c^{(k)}$ and optimize it in the neighborhood of $\boldsymbol{x}^{(K)}$ defined as $[\boldsymbol{x}^{(K)} - d, \boldsymbol{x}^{(K)} + d]$, where $d = [d_1\ d_2 \ldots d_n]^T$. The size of the neighborhood can be selected based on sensitivity analysis of c_1 (the cheapest of the low-fidelity models); usually d equals 2 to 5 percent of $\boldsymbol{x}^{(K)}$.

Here, approximation is performed using a reduced quadratic model $q(\boldsymbol{x}) = [q_1\ q_2 \ldots q_m]^T$, defined as

$$q_j(\boldsymbol{x}) = q_j([x_1 \ldots x_n]^T) = \lambda_{j.0} + \lambda_{j.1}x_1 + \ldots + \lambda_{j.n}x_n + \lambda_{j.n+1}x_1^2 + \ldots + \lambda_{j.2n}x_n^2 \tag{2}$$

The coefficients $\lambda_{j.r}$, $j = 1, \ldots, m$, $r = 0, 1, \ldots, 2n$, are uniquely obtained by solving the linear regression problems

$$\begin{bmatrix} 1 & x_{-n.1}^{(K)} & \cdots & x_{-n.n}^{(K)} & (x_{-n.1}^{(K)})^2 & \cdots & (x_{-n.n}^{(K)})^2 \\ \vdots & \vdots & & \vdots & & \vdots & \vdots \\ 1 & x_{0.1}^{(K)} & \cdots & x_{0.n}^{(K)} & (x_{0.1}^{(K)})^2 & \cdots & (x_{-n.n}^{(K)})^2 \\ \vdots & \vdots & & \vdots & & \vdots & \vdots \\ 1 & x_{n.1}^{(K)} & \cdots & x_{n.n}^{(K)} & (x_{n.1}^{(K)})^2 & \cdots & (x_{-n.n}^{(K)})^2 \end{bmatrix} \cdot \begin{bmatrix} \lambda_{j.0} \\ \lambda_{j.1} \\ \vdots \\ \lambda_{j.2n} \end{bmatrix} = \begin{bmatrix} c_j^{(-n)} \\ \vdots \\ c_j^{(0)} \\ \vdots \\ c_j^{(n)} \end{bmatrix} \tag{3}$$

where $\boldsymbol{x}_{k.j}^{(K)}$ is a jth component of the vector $\boldsymbol{x}_k^{(K)}$, and $c_j^{(k)}$ is a jth component of the vector $c^{(k)}$. In our case, the components of the response vector consist of the lift and drag coefficients, as well as the cross-section area.

In order to account for unavoidable misalignment between c_K and f, instead of optimizing the quadratic model q, it is recommended to optimize a corrected model $q(\boldsymbol{x}) + [f(\boldsymbol{x}^{(K)}) - c_K(\boldsymbol{x}^{(K)})]$ that ensures a zero-order consistency [6] between c_K and f. The refined design can be then found as

$$\boldsymbol{x}^* = \arg\min_{\boldsymbol{x}^{(K)} - d \le \boldsymbol{x} \le \boldsymbol{x}^{(K)} + d} H(q(\boldsymbol{x}) + [f(\boldsymbol{x}^{(K)}) - c_K(\boldsymbol{x}^{(K)})]) \tag{4}$$

This kind of correction is also known as output space mapping [13]. If necessary, the step (4) can be performed a few times starting from a refined design, i.e., $\boldsymbol{x}^* = \text{argmin}\{\boldsymbol{x}^{(K)} - d \le \boldsymbol{x} \le \boldsymbol{x}^{(K)} + d : H(q(\boldsymbol{x}) + [f(\boldsymbol{x}^*) - c_K(\boldsymbol{x}^*)])\}$. It should be noted that the high-fidelity model is not evaluated until executing the refinement step (4). Also, each refinement-iteration requires only a single evaluation of f.

The optimization procedure can be summarized as follows (where K is the number of models):

1. Set $j = 1$;
2. Select the initial design $\boldsymbol{x}^{(0)}$;
3. Starting from $\boldsymbol{x}^{(j-1)}$ find $\boldsymbol{x}^{(j)} = \arg\min\{\boldsymbol{x} : H(c_j(\boldsymbol{x}))\}$;
4. Set $j = j + 1$; if $j < K$ go to 3;
5. Obtain a refined design according to (4).

The main benefit of using models of different fidelity is that starting from a less accurate but faster model allows us to quickly find an approximate location of the optimum design. Switching to finer models at the later stages allows us to locate the optimum more accurately without excessive computational effort because each algorithm-iteration starts from an already reasonable approximation of the optimum. Another benefit of this procedure is that, aside from the refinement stage, no enhancement/correction of the low-fidelity models is necessary, which is in contrast to most of other SBO techniques. Therefore, the multi-level approach is less dependent on the low-fidelity model quality.

3. High-fidelity CFD Model

Two-dimensional transonic flow past airfoil sections is considered. The flow is assumed to be steady, inviscid, and adiabatic, with no body forces. The compressible Euler equations are taken to be the governing fluid flow equations.

3.1. Computational Grid

The computational domain is shown in Fig. 1a. The free-stream Mach number, static pressure, and angle of attack are prescribed at the farfield boundary. The solution domain boundaries are placed at 25 chord lengths in front of the airfoil, 50 chord lengths behind it, and 25 chord lengths above and below it. The computational grids are of structured curvilinear body-fitted C-topology with elements clustering around the airfoil and growing in size with distance from the airfoil surface.

The grid density is controlled by the following parameters: m_1 = number grid points on the upper and lower airfoil surfaces, m_2 = number grid points on the horizontal line behind the airfoil from the trailing-edge to the farfield boundary, m_3 = number of grid points on the vertical line from the airfoil surface to one-fourth of the distance to the farfield, m_4 = number of grid points on the three-fourths of the vertical line from the farfield down to the airfoil surface, and m_5 = distance from the airfoil surface to the first grid point. Local clustering on the airfoil surface is also controlled, but not parameterized. The computer code ICEM CFD [14] is used for the grid generation. An example grid is shown in Fig. 1b.

3.2. Flow Solver

Numerical fluid flow simulations are performed using the computer code FLUENT [15]. The flow solver is of implicit density-based formulation and the inviscid fluxes are calculated by an upwind-biased second-order spatially accurate Roe flux scheme. Asymptotic convergence to a steady state solution is obtained for each case. The iterative convergence of each solution is examined by monitoring the overall residual, which is the sum (over all the cells in the computational domain) of the L^2 norm of all the governing equations solved in each cell. The solution convergence criterion for the high-fidelity model is the one that occurs first of the following: a maximum residual of 10^{-6}, or a maximum number of iterations of 1000.

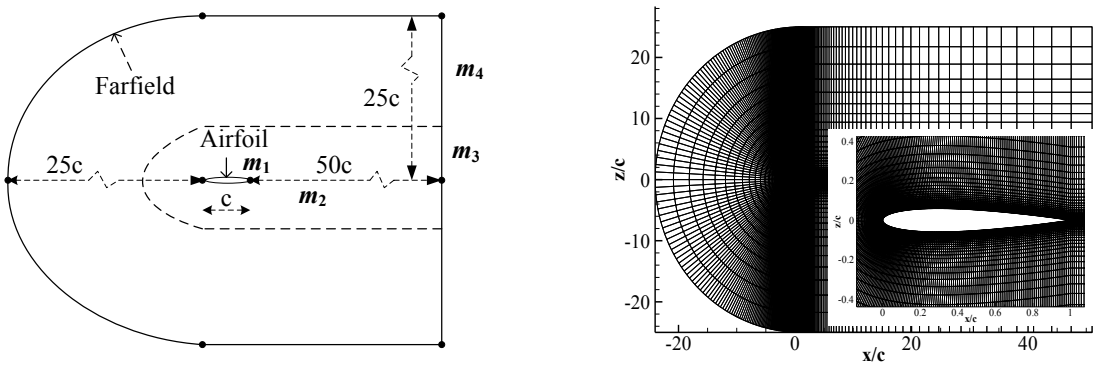

(a) (b)

Fig. 1. Structured curvilinear body-fitted C-topology grid for transonic airfoil flow simulation, (a) the computational domain, and (b) an example grid for the NACA 0012 airfoil.

3.3. Grid Independence

A grid independence study was performed using the NACA 0012 airfoil at Mach number $M_\infty = 0.75$ and angle of attack $\alpha = 1°$. The study, shown in Fig. 2a, revealed that 407,676 mesh cells are needed for mesh convergence, and that particular mesh was used for the high-fidelity model. The overall simulation time for the case considered is around 67 minutes (Fig. 2b). The flow solver reached a converged solution after 352 iterations. The other meshes required around 350 to 500 iterations to converge, except the coarsest mesh, which terminated after 1000 iterations, with the overall simulation time around 9.5 minutes.

4. Low-fidelity CFD Models

The low-fidelity CFD models are constructed in the same way as the high-fidelity model, but with a coarser computational mesh and relaxed convergence criteria. As explained in Section 2, the optimization algorithm presented here may exploit several models of different fidelity. Setup of the low-fidelity CFD models is of utmost importance for the performance and efficiency of the multi-fidelity optimization algorithm.

The grid density is controlled by five parameters, m_i, $i = 1,\ldots,5$, as described in Section 3.1. The number of flow solver iterations is denoted by N. The vector of all combined parameters will be referred to as $\boldsymbol{z} = [m_1\ m_2\ m_3\ m_4\ m_5\ N]$. In this work, we consider three different ways of setting up these parameters in order to setup the low-fidelity models for the multi-level optimization algorithm, as well as their influence on the algorithm performance.

4.1. Low-Fidelity Model Setup based on Grid Independence Study

The most common strategy for setting up the low-fidelity models is by using the results of a grid independence study. The process is typically done in "reverse", meaning a high-fidelity grid is developed by an experienced engineer and then the number of grid points in each direction is reduced by half. The distance to the first grid point is doubled as well. Figure 2 is an example of such study.

The flow solution history, shown in Fig. 3a, for a low-fidelity model indicates that the lift and drag coefficients are nearly converged after 80 to 100 iterations. The maximum number of iterations is set to 100 for the low-fidelity model. This reduces the overall simulation time further. A comparison of the pressure distributions of the high- and the low-fidelity models, shown in Fig. 3b, indicates that the low-fidelity model, in spite of being based on much coarser mesh and reduced flow solver iterations, captures the main features of the high-fidelity model pressure distribution quite well. The biggest discrepancy in the distributions is around the shock on the upper surface, leading to an over estimation of both lift and drag (Fig. 2a).

4.2. Low-Fidelity Model Setup based on Insight

An alternative way of setting up the low-fidelity models is by modifying the grid parameters based on the insight of the engineer. The objective would be to reduce the simulation time, but at the same time retain the accuracy of the high-fidelity model. For example, regions with large gradients need to be resolved better than other regions. With that in mind, one can reduce the number of grid points in the outer regions more than in the region close to the airfoil surface. In our case, the grid parameters m_2 and m_4 can be reduced more rapidly than the other grid parameters. The number of flow solver is set in the same way as described in Section 4.1.

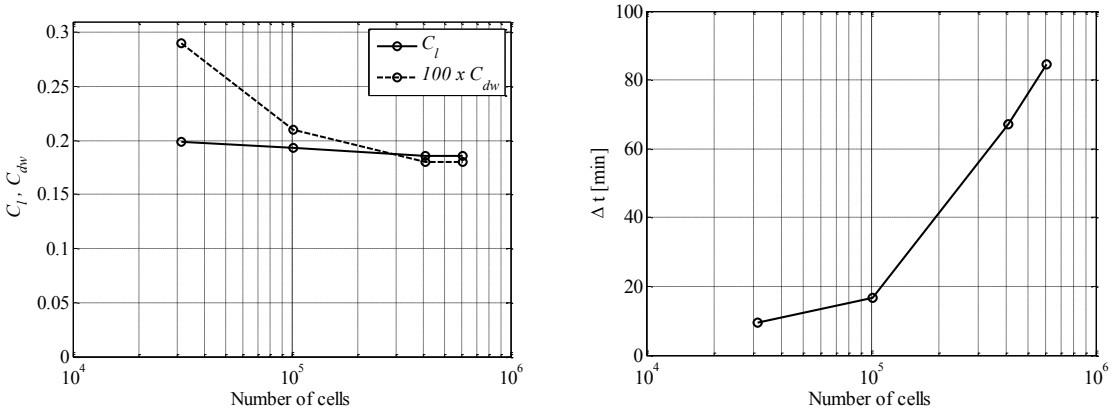

(a) (b)

Fig. 2. Grid independence study using the NACA 0012 airfoil at Mach number M_∞ = 0.75 and angle of attack α = 1°; (a) lift and drag coefficients versus the number mesh cells, and (b) the simulation time versus the number of mesh cells.

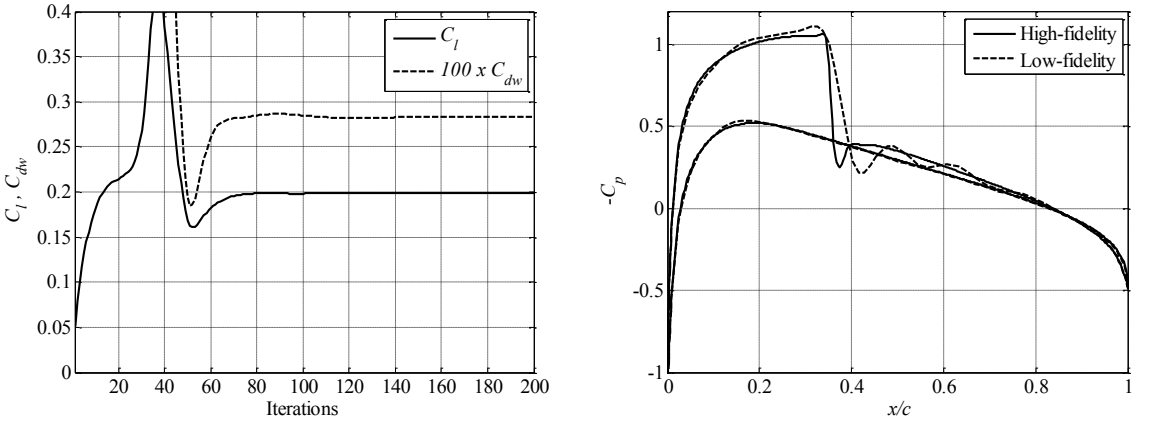

(a) (b)

Fig. 3. Simulation results for NACA 0012 at Mach number M_∞ = 0.75 and angle of attack α = 1°; (a) evolution of the lift and drag coefficients obtained by the "coarser" low-fidelity model in Fig.2; (b) comparison of the pressure distributions obtained by the high- and low-fidelity models.

4.3. Low-Fidelity Model Setup based on Numerical Optimization

The last low-fidelity model setup methodology considered here exploits numerical optimization. More specifically, the grid parameters as well as the number of iterations N, i.e., the vector $\boldsymbol{z}$, are optimized in order to reduce the discrepancy between the drag coefficients predicted by the low-fidelity model and the high-fidelity one, assuming given simulation time ratios between the models. Let us denote the drag coefficient predicted by a CFD model simulated using the grid/iteration parameters $\boldsymbol{z}$ as $C_d(\boldsymbol{x},M,\alpha,\boldsymbol{z})$, where $\boldsymbol{x}$ represents the airfoil geometry, whereas M and α are operating conditions (Mach number and angle of attack) for a reference airfoil for which the low-fidelity model is being set up. The optimization problem is defined as follows

$$z^* = \arg\min_z H_z(C_d(\boldsymbol{x}, M, \alpha, z)) \tag{7}$$

with the objective function defined as

$$H_z(C_d(\boldsymbol{x}, M, \alpha, z)) = \left(\frac{C_d(\boldsymbol{x}, M, \alpha, z) - C_d(\boldsymbol{x}, M, \alpha, z_f)}{C_d(\boldsymbol{x}, M, \alpha, z_f)} \right)^2 + \gamma \left(\frac{t(z_f)}{t(z)} - R_{\text{target}} \right)^2 \tag{8}$$

Here, z_f are grid parameters for the high-fidelity model, $C_d(\boldsymbol{x},M,\alpha,z_f)$ is the drag coefficient predicted by the high-fidelity model for the reference airfoil and operating conditions, whereas $t(z)$ represents the CFD model simulation time for given grid parameters z. The objective function contains the penalty factor with the proportionality coefficient γ (here, we use γ = 1000) that forces the optimization process to obtain given simulation time ratio R_{target}.

The low-fidelity model setup through the optimization process (7), (8) allows us to obtain the best possible grid setup for a required simulation time ratio that can be controlled much more precisely than for the typical methods of Sections 4.1 and 4.2. As demonstrated in Section 5, this is directly translated into a better efficiency of the multi-level optimization algorithm.

5. Numerical Results

The multi-fidelity optimization algorithm, described in Section 2, is applied to the design of a transonic airfoil section. The high-fidelity model is described in Section 3. Three different optimization runs are performed, each with different setup of the low-fidelity models (cf. Section 4). Two low-fidelity models are used in each optimization run.

5.1. Families of Low-fidelity Models

The NACA 0012 airfoil shape was selected as a baseline and three families of low-fidelity models were generated at M_∞ = 0.75 and α = 1°. The families are denoted as LFM 1 = linear variation of all grid parameters (cf. Section 4.1), LFM 2 = variation of a set of grid parameters (cf. Section 4.2), and LFM 3 = numerical optimization of the grid parameters (cf. Section 4.3).

The results are shown in Fig. 4. It can be seen that the lift coefficient values (Fig. 4a) diverge from the high-fidelity value as the grid cells are reduced for all the low-fidelity model families. However, the drag coefficient values (Fig. 4b) diverge from the high-fidelity one as the cell number is reduced for both LFM 1 (constructed by a typical grid independence study) and LFM 2 (constructed by insight), but not for LFM 3 (constructed by numerical optimization) which stays nearly constant with respect to the number of cells. Moreover, the time ratio (Fig. 4c) increases more rapidly with reduced number of cells for the LFM 3 family than the other two. Thus, it seems that constructing the low-fidelity model families using numerical optimization yields both more accurate and faster models.

5.2. Airfoil Shape Optimization

The multi-level optimization algorithm of Section 2.2 is applied to airfoil shape optimization of a design case involving drag minimization. The pattern-search algorithm, a derivative-free optimization method (see, e.g., Ref. 12), is used for the low-fidelity model optimization (Step 3 of the algorithm). The airfoil shape is parameterized using the NACA four-digit airfoil with m (the maximum ordinate of the mean camberline as a fraction of chord), p (the chordwise position of the maximum ordinate), and t/c (the thickness-to-chord ratio) as the design variables (see Abbott and von Doenhoff[32] for details).

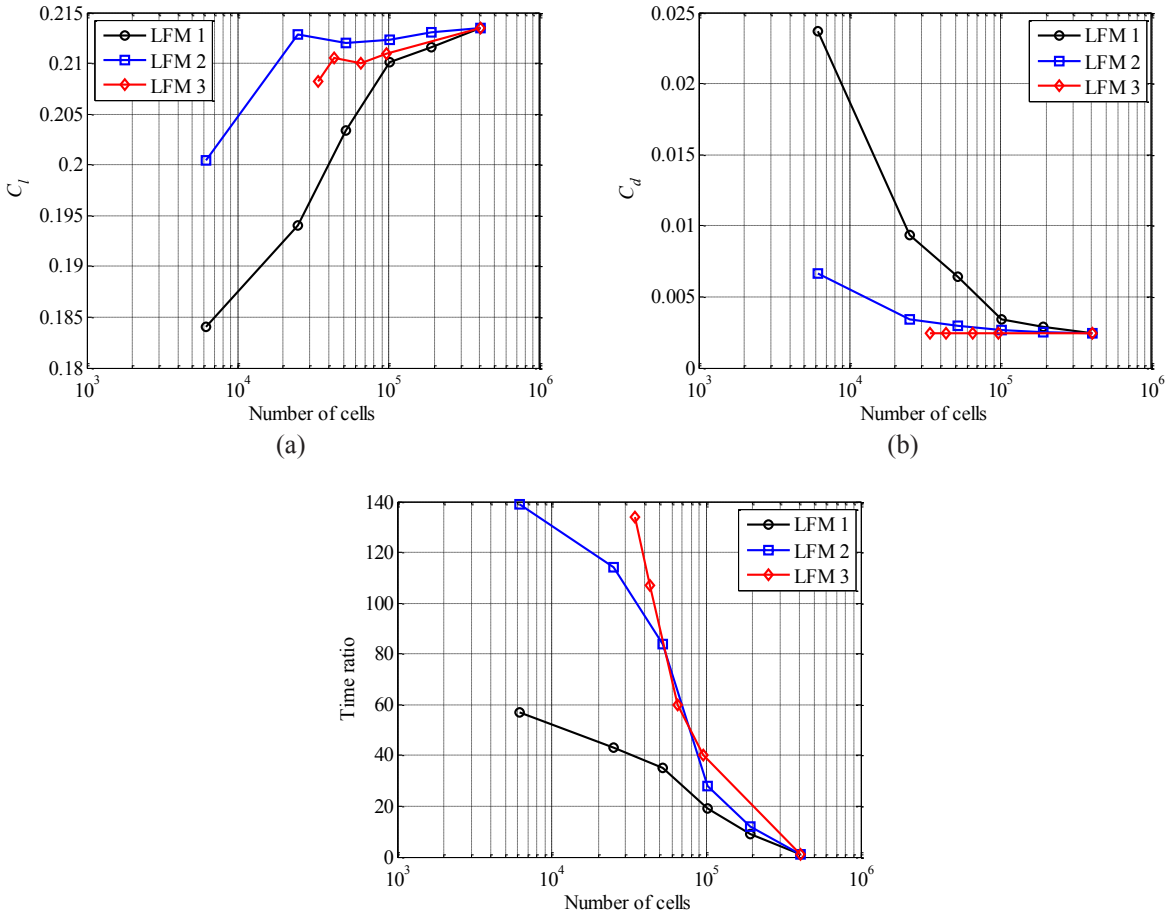

Fig. 4. Numerical results of three different ways of low-fidelity model setup (NACA 0012, $M_\infty = 0.75$, $\alpha = 1°$). Shown are the variations of (a) the lift coefficient, (b) drag coefficient, and (c) ratio of the high-to-low-fidelity simulation time with the number of grid cells.

Table 1. Simulation time ratio for the high-to-low-fidelity models for each low-fidelity model used from different families.

Model	LFM 1	LFM 2	LFM 3
c_1	25	84	100
c_2	3	12	40

Table 2. Numerical results of optimization using three different low-fidelity model families.

Variable	Initial	LFM 1	LFM 2	LFM 3
m	0.0200	0.0175	0.0166	0.0180
p	0.4000	0.5500	0.5800	0.5233
t	0.1200	0.1114	0.1164	0.1114
C_l	0.4745	0.6001	0.6000	0.6000
C_{dw}	0.0115	0.0016	0.0018	0.0017
A	0.0808	0.0750	0.0784	0.0751
N_{c1}	–	51	54	52
N_{c2}	–	38	38	38
N_f	–	3	3	2
Cost	–	< 18	< 7	< 4

Three optimization studies are performed using the three different low-fidelity model familes constructed in the previous section. Two low-fidelity models are used by the multi-level optimization algorithm. Table 1 shows the time ratio of the two low-fidelity models used from each family. Using faster models for LFM 1 and LFM 2 either resulted in failed simulations during the optimization run, i.e., the grids were simply to coarse for the flow solver to handle, or the optimizer would not yield improved designs.

The objective is to minimize the wave drag coefficient (C_{dw}) subject to a constraint on the lift coefficient ($C_{l.min}$ = 0.6) and the non-dimensional cross-sectional area (A_{min} = 0.075). The bounds on the design variables are $0 \le m \le 0.1$, $0.2 \le p \le 0.8$, and $0.05 \le t/c \le 0.2$. The Mach number is $M_\infty = 0.75$ and the angle of attack $\alpha =$ 1°. Details of the optimization results are given in Table 2.

The results for this particular design case show that the optimized designs obtained by using the three different low-fidelity model families are similar. The thickness-to-chord ratio is nearly the same for all designs, but the maximum camber and the location of maximum camber differ slightly. All designs satisfy both constraints, but they differ slightly in the objective function (by one drag count, which is 0.0001 of the drag coefficient value).

The number of function calls to the low-fidelity models (N_{c1} and N_{c2}) is also similar for all families. The number of function calls to the high-fidelity model for LFM 1 and LFM 2 are 3, but 2 for LFM 3. However, the overall cost, in terms of equivalent high-fidelity function calls, is less than 18 for LFM 1, less than 7 for LFM 2, and less than 4 for LFM 3; which is due to the difference in the speed of the low-fidelity models (cf. Table 1).

6. Conclusion

An automated low-fidelity model selection technique for variable-resolution surrogate-based optimization is presented. The technique replaces a hands-on process guided by experience to yield accurate and reliable low-fidelity models. A design optimization application indicates that the proposed approach can yield significant computational savings when compared to the conventional way of setting up low-fidelity models. Future work will be focused on reliability issues. In particular, generating discretization parameters based on multiple airfoil shapes will be considered, which is expected to improve of the low-fidelity models in terms of consistent prediction of aerodynamic forces (with respect to the high-fidelity model) across the design space.

References

1. Leoviriyakit, K., Kim, S., and Jameson, A., "Viscous Aerodynamic Shape Optimization of Wings including Planform Variables," *21st Applied Aerodynamics Conference*, Orlando, Florida, June 23-26, 2003.
2. Braembussche, R.A., "Numerical Optimization for Advanced Turbomachinery Design," In *Optimization and Computational Fluid Dynamics*, Thevenin, D. and Janiga, G., editors, Springer, 2008, pp. 147-189.
3. Queipo, N.V., Haftka, R.T., Shyy, W., Goel, T., Vaidyanathan, R., and Tucker, P.K., "Surrogate-Based Analysis and Optimization," *Progress in Aerospace Sciences*, Vol. 41, No. 1, 2005, pp. 1-28
4. Forrester, A.I.J., and Keane, A.J., "Recent advances in surrogate-based optimization," *Progress in Aerospace Sciences*, Vol. 45, No. 1-3, 2009, pp. 50-79.
5. S. Koziel, D. Echeverría-Ciaurri, and L. Leifsson, "Surrogate-based methods," in S. Koziel and X.S. Yang (Eds.) *Computational Optimization, Methods and Algorithms*, Series: Studies in Computational Intelligence, Springer-Verlag, pp. 33-60, 2011.
6. Alexandrov, N.M., Lewis, R.M., Gumbert, C.R., Green, L.L., and Newman, P.A., "Optimization with Variable-Fidelity Models Applied to Wing Design," *38th Aerospace Sciences Meeting & Exhibit*, Reno, NV, AIAA Paper 2000-0841, Jan. 2000.
7. Robinson, T.D., Eldred, M.S., Willcox, K.E., and Haimes, R., "Surrogate-Based Optimization Using Multifidelity Models with Variable Parameterization and Corrected Space Mapping," *AIAA Journal*, vol. 46, no. 11, 2008.
8. Booker, A.J., Dennis Jr., J.E., Frank, P.D., Serafini, D.B., Torczon, V., and Trosset, M.W., "A rigorous framework for optimization of expensive functions by surrogates," *Structural Optimization*, Vol. 17, No. 1, 1999, pp. 1-13.
9. Barrett, T.R., Bressloff, N.W., and Keane, A.J., "Airfoil Design and Optimization Using Multi-Fidelity Analysis and Embedded Inverse Design," AIAA Paper 2006-1820, *47th AIAA/ASME/ASCE/AHS/ASC Structures, Structural Dynamics, and Materials Conference*, Newport, Rhode Island, 2006.

10. Leifsson, L., and Koziel, S., "Multi-fidelity design optimization of transonic airfoils using physics-based surrogate modeling and shape-preserving response prediction," *Journal of Computational Science*, Vol. 1, No. 2, 2010, pp.98-106.
11. Koziel, S., and Leifsson, L., "Multi-level surrogate-based airfoil shape optimization," 51st *AIAA Aerospace Sciences Meeting including the New Horizons Forum and Aerospace Exposition*, Grapevine, Texas, January 7-10, 2013.
12. Koziel, S., "Multi-fidelity multi-grid design optimization of planar microwave structures with Sonnet," *International Review of Progress in Applied Computational Electromagnetics*, Tampere, Finland, April 26-29, 2010, pp. 719-724.
13. S. Koziel, Q.S. Cheng, and J.W. Bandler, "Space mapping," *IEEE Microwave Magazine*, vol. 9, no. 6, pp. 105-122, Dec. 2008.
14. ICEM CFD, ver. 14.0, ANSYS Inc., Southpointe, 275 Technology Drive, Canonsburg, PA 15317, 2010.
15. FLUENT, ver. 14.0, ANSYS Inc., Southpointe, 275 Technology Drive, Canonsburg, PA 15317, 2010.